Front. Struct. Civ. Eng. 2025, 19(6): 859–871
https://doi.org/10.1007/s11709-025-1188-1

RESEARCH ARTICLE

Frost heaving behavior and mechanical deterioration of prestressed concrete

Xiguang LIU[a,b*], Huimin ZHANG[a], Jingxi PENG[c], Yao LV[a], Ditao NIU[a]

[a] *College of Civil Engineering, Xi'an University of Architecture and Technology, Xi'an 710055, China*
[b] *Institute for Interdisciplinary and Innovate Research, Xi'an 710055, China*
[c] *Beijing YJK Building Software Co., Ltd., Beijing 100013, China*
[*] *Corresponding author. E-mail: xgliu@xauat.edu.cn*

ABSTRACT Freeze–thaw (FT) damage can cause frost heaving and cracking of prestressed concrete (PC) structures, and a decrease in the strain of prestressing tendon, which seriously affects the safety of the structures. An experimental study was conducted to investigate the frost heaving behavior and mechanical deterioration of bonded post-tensioned PC components in an FT environment. The strain variations along the length of the components during 300 freeze–thaw cycles (FTCs) were obtained, and the effects of FTCs and stress levels on concrete frost heaving strain and prestressing tendon strain loss were analyzed. The results indicated that with increasing FTCs, the concrete frost heaving strain, the residual strain, and the loss of the prestressing tendon strain all increased. As the stress level rose, the effect of prestress forces on the concrete frost cracking from inhibition switched to aggravation. Considering the effects of FTCs and stress levels, a strain loss model for the components was established, and it was in good agreement with the experimental results.

KEYWORDS prestressed concrete components, freeze–thaw cycles, stress level, frost heaving strain

1 Introduction

Freeze–thaw cycles (FTCs) can cause frost heaving and cracking in concrete. In cold regions, FTCs are one of the primary factors compromising the durability of concrete structures [1–3]. Prestressed concrete (PC) structures are widely employed for their superior crack resistance [4]. However, they are vulnerable to FTC-induced prestressing tendon strain loss. The degradation reduced effective tensile stress, severely impacting structural safety [5,6].

Experimental research on the mechanical properties of concrete materials and PC components under FTCs has been conducted. The test results demonstrated that as FTCs progressed, the concrete's relative dynamic modulus of elasticity and compressive strength declined progressively [7–9]. The cracking load of the PC components showed a linear decreasing trend, with a reduction in stiffness and development of surface cracks, and the prestressing tendon strain exhibited a consistent reduction [10–12].

The frost heaving behavior of concrete during FTCs has been tested [13–15]. During freezing, pore water within concrete froze and expanded, generating frost heaving strain through pressure exerted on the cementitious matrix [16,17]. During thawing, water persistently migrated and caused residual strain, which was essentially the plastic deformation of the concrete [18]. As the number of FTCs increased, residual deformation in concrete accumulated [19–21], demonstrating that FTC-induced deterioration was a cumulative and irreversible degradation mechanism [22].

A few studies have been focused on the concrete frost resistance under coupled mechanical loading and FTCs [23,24]. The combined effects of FTCs and uniaxial compressive loads degraded both mechanical properties and frost resistance of concrete [25,26]. The experimental results revealed that a stress level below 0.3 f_c could delay the occurrence of frost heaving and cracking of PC components, while a higher stress level (greater than 0.5

Article history: Received Oct 9, 2024; Accepted Mar 10, 2025

f_c) could aggravate the development of micro-cracks, facilitating water penetration and subsequent frost resistance deterioration [27].

Bonded PC components are interconnected by grouting, which ensures the bond between the prestressing tendon and the concrete. However, FTCs caused degradation at the grout-concrete-tendon interface [28]. Under the influence of FTCs, the damage to the bond interface varied along the length of the components, leading to different patterns of prestressing tendon strain loss along the length.

Previous studies have predominantly focused on the durability deterioration behavior and material degradation mechanisms of structures under single environmental conditions or loading effects. Although limited research has been conducted on PC structures in freeze–thaw (FT) environments, existing investigations have primarily concentrated on macroscopic performance degradation and prestress loss, with insufficient exploration of concrete frost heaving strain and prestressing tendon strain. Furthermore, the strain development patterns along the bond direction after FT-induced damage have not been fully understood.

The FT tests of bonded post-tensioned PC components were conducted, and the effects of FTCs and stress levels on the frost heaving strain and the prestressing tendon strain were studied. The influence of the strains development at different positions of the components was analyzed. Based on the deformation coordination principle, a strain loss model of PC components under FTCs was established and was acceptable with experimental results.

2 Experimental procedure

2.1 Components design

Eight bonded post-tensioned PC components were designed and fabricated. The length of each component was 2000 mm and the cross-sectional dimension was 100 mm × 100 mm, as shown in Fig. 1. The stress levels of the components were 0.1, 0.2, 0.3, and 0.4, sequentially representing the tensile stress as 10%, 20%, 30%, and 40% of the average compressive strength of the concrete. The numbers of FTCs were 0, 50, 100, 150, 200, 250, and 300.

The measured compressive strength of concrete cubes with strength grade C40 in 28 d was 37.14 MPa. Table 1 presents the concrete mix design. The PC components were cured for 28 d in the condition with a temperature of (20 ± 2) °C and a relative humidity greater than 95%.

The grouting material for the ducts was Class I, following the Technical Code for the Application of Cementitious Grout (GB/T 50448-2015) [29]. The ratio of water-cement was 0.32. The measured compressive strength in 28 d was 59.30 MPa.

The high-strength bars were prestressing screw bars of 830 grade, with a diameter of 18, a measured yield strength of 918 MPa, an elastic modulus of 2.11 × 10^5 MPa, and an elongation of 15%.

2.2 Components fabrication

The post-tensioned PC components had a duct diameter of 26 mm and were formed using the steel pipe coring method. After curing the components, the prestressing tendons were tensioned using the devices shown in Fig. 2. The strain gauges were attached to both the surface of the concrete and the prestressing tendon to record strain. The arrangement of the strain gauges is shown in Fig. 1. The design and actual stress levels of the components are shown in Table 2. After tensioning the PC components, grouting was carried out through the holes.

3 Test method

3.1 Freeze–thaw test

The FT tests were conducted by the Standard for Test Methods of Long-term Performance and Durability of

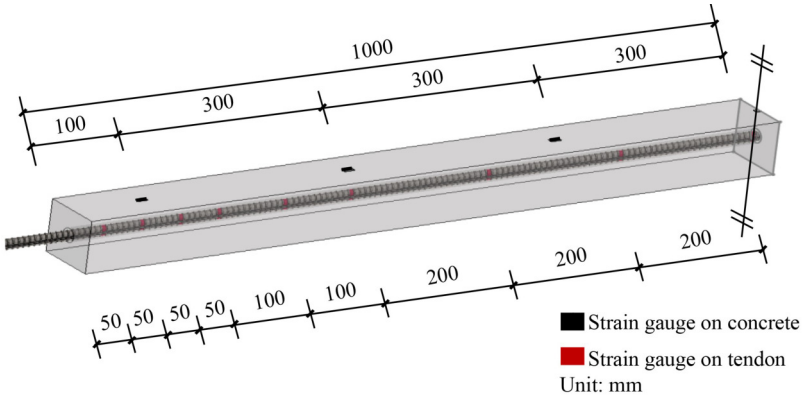

Fig. 1 Dimension of components and arrangement of strain gauges (mm).

Table 1 Concrete mix design

w/c	Cement (kg/m^3)	Water (kg/m^3)	Fine aggregate (kg/m^3)	Coarse aggregate (kg/m^3)	Enhancing agent (%)	Water-reducing agent (%)
0.33	327	138	781	1100	5.15	7.8

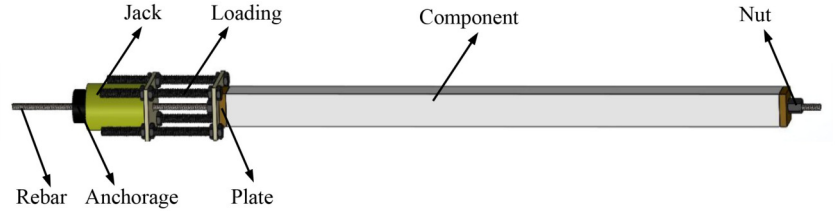

Fig. 2 Tensioning devices for components.

Table 2 Stress levels of the components

Component	Test environment	Design stress level	Actual stress level
C1	T = (−20–25) °C; Relative Humidity (RH) > 95%	0.1	0.11
C2	T = (−20–25) °C; RH > 95%	0.2	0.22
C3	T = (−20–25) °C; RH > 95%	0.3	0.31
C4	T = (−20–25) °C; RH > 95%	0.4	0.41
C5	T = (20 ± 2) °C; RH > 95%	0.1	0.13
C6	T = (20 ± 2) °C; RH > 95%	0.2	0.20
C7	T = (20 ± 2) °C; RH > 95%	0.3	0.37
C8	T = (20 ± 2) °C; RH > 95%	0.4	0.47

Ordinary Concrete (GB/T 50082-2009) [30]. After being cured for 24 d, the components were immersed in water at a temperature of (20 ± 2) °C for 4 d, with the water level 20–30 mm above the top surface of the concrete. After immersion, the components were taken out, tensioned, grouted, and cured before FT tests. The FT tests were divided into four stages, including a two-hour cooling period from 25 to −20 °C, followed by a two-hour low-temperature constant period, then a one-hour warming period from −20 to 25 °C, and finally a one-hour constant temperature period. Three cycles of spraying were performed after the end of the final period, marking the completion of one full FTC.

The control group components, which were not subjected to FTCs, were placed in an environment with a temperature of (20 ± 2) °C and humidity greater than 95%. To ensure insulation and moisture retention, the concrete components were wrapped in sponges and sprayed regularly.

3.2 Ultrasonic test

The ultrasonic propagation velocity of the PC components before and after FT tests was measured following the Technical Specification for the Inspection of Concrete Defects by Ultrasonic Method (CECS21-2000) [31]. The relationship between dynamic modulus of elasticity (E_d) and ultrasonic propagation velocity is shown in Eq. (1) [32].

$$E_d = \frac{2(1+\mu)^3}{(0.87+1.12\mu)^2}\rho V_r^2, \tag{1}$$

where μ is concrete Poisson's ratio; ρ is concrete density, kg/m^3; V_r is concrete ultrasonic propagation velocity, km/s.

The effects of changes in Poisson's ratio and density were not considered during the FT tests. The concrete relative dynamic modulus of elasticity (E_{rd}) is calculated using Eq. (2), and then used the variation of E_{rd} to assess the FT damage of the components.

$$E_{rd} = \frac{V_N^2}{V_0^2} \times 100\%, \tag{2}$$

where V_N is the ultrasonic propagation velocity of the concrete under FTCs, km/s; V_0 is the ultrasonic propagation velocity of the unfrozen concrete, km/s.

3.3 Strain test

The total strain of the prestressing tendon during the tests included the strain generated during the tensioning process, the frost heaving strain resulting from the freezing and expansion of pore water during the FTCs, and the thermal strain caused by thermal expansion and contraction. The thermal and frost heaving strains were induced during the FT test [33]. To eliminate the influence of thermal expansion and contraction, a dynamic simulation method was employed to compensate for temperature and eliminate the thermal strain [34,35]. Strain gauges, one for compensation and the other for testing, were attached to components made of the same material. The specimens and strain gauges used for compensation were waterproofed. By subtracting the compensated strain from the tested strain, the frost heaving strain was determined. The frost heaving strain ε_f can be calculated using Eq. (3)

$$\varepsilon_f = \varepsilon_i - \varepsilon_t - \varepsilon_s, \tag{3}$$

where ε_i is the total strain of the prestressing tendon; ε_t is

the thermal strain; ε_s is the strain generated during the tensioning process.

The variations of the concrete frost heaving strain and the total strain of the prestressing tendon are shown in Fig. 3. As shown, with the decline in the temperature, the total strain decreased, while the frost heaving strain ascended accordingly. The total strain loss of the prestressing tendon can be calculated by Eq. (4)

$$\Delta\varepsilon = \varepsilon - \varepsilon_N, \tag{4}$$

where $\Delta\varepsilon$ is the total strain loss; ε is the total strain before the FT tests; ε_N is the total strain after N FTCs.

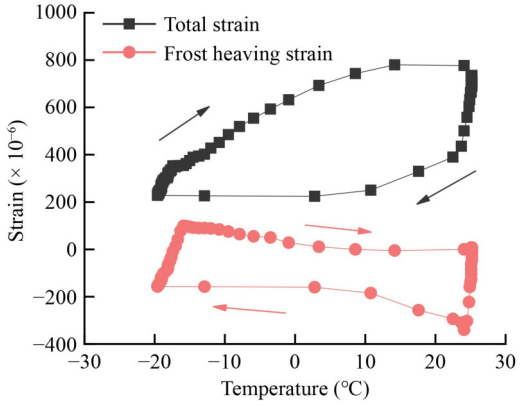

Fig. 3 Variations of the total strain and frost heaving strain.

4 Results and discussion

4.1 Analysis of concrete surface morphology

The surface morphology of the PC components during FTCs is shown in Fig. 4. It can be seen that with increasing FTCs and stress levels, the surface cracks of the components increased, the width of cracks widened, and eventually the cracks intersected and penetrated, leading to concrete surface peeling. After the FT tests, the stress levels of the components ranged from 0.1 to 0.4, the number of frost heaving cracks were 7, 8, 12, and 13, respectively, and the maximum crack widths were 0.35, 0.38, 12, and 10 mm.

The interface damage of the components was observed after the FT tests, as shown in Fig. 5. It indicates that the interface damage between the grouting material, PC and prestressing tendon worsened progressively with increasing stress levels. For components with higher stress levels of 0.3 and 0.4, the concrete surface peeled off, exposing the prestressing tendon.

The phenomenon was attributed to inherent defects in the concrete material. As FTCs progressed, the pre-existing voids within the concrete underwent repeated processes of water freezing and expansion. It led to the progressive development of microcracks, which eventually evolved into visible surface cracks. Moreover, the interfacial transition zone between the prestressing tendon and the concrete is one of the weakest areas in the structure. FT-induced microcracks tended to propagate preferentially within this zone, weakening the mechanical bonding and compromising the integrity of the interface.

4.2 Analysis of concrete mechanical properties

Figure 6 exhibits the mechanical properties of concrete cubes and PC components with FTCs. It can be indicated that with the increase of FTCs, the loss rate of the compressive strength ascended accordingly. After 250 FTCs, the compressive strength loss rate reached 64.2%.

As the number of FTCs increased, the variations in the E_{rd} of the components under different stress levels steadily decreased. The higher the stress level, the faster the rate of loss in E_{rd}. For the component with a stress level of 0.3, the appearance of larger cracks during the loading process led to significantly higher internal damage compared to the other components. After 200 FTCs, the E_{rd} with stress levels of 0.1, 0.2, 0.3, and 0.4 decreased by 19.0%, 21.6%, 72.6%, and 44.8%, respectively.

As demonstrated in Subsection 4.1, FTCs induced the propagation of internal cracks and the deterioration of the bond interface within the components. The loosening of the pore structure compromised the load-bearing capacity, which was macroscopically reflected as a decrease in compressive strength. Microcracks hindered the stress transfer paths, resulting in a decline in ultrasonic propagation velocity and, consequently, a reduction in the dynamic modulus of elasticity.

4.3 Analysis of the prestressing tendon strain

4.3.1 The total strain of unfrozen components

The variations of the total strain with time for the comparison group components in ambient temperature were obtained, as shown in Fig. 7. The total strain showed no significant change during the tests, with an approximately linear variation.

4.3.2 Effects of freeze–thaw cycles

Figure 8 shows the variations of the total strain loss with FTCs. It can be observed that with the increase in FTCs, the total strain loss under various stress levels rose.

For components with stress levels of 0.1 and 0.2, the total strain loss developed rapidly before 50 FTCs, and then entered a steady growth phase. After 200 FTCs, the loss entered an unstable development stage and exhibited exponential growth.

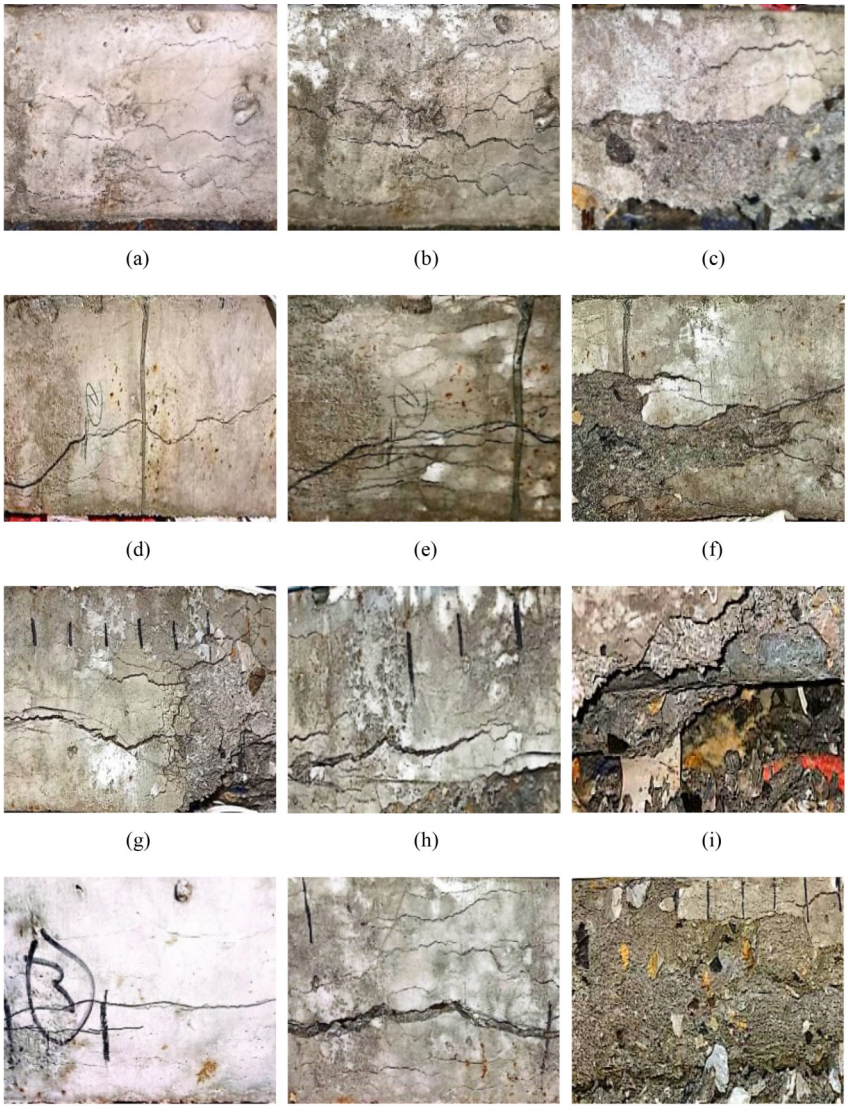

Fig. 4 Damage development of the component surface: (a) $m = 0.1$, $N = 100$; (b) $m = 0.1$, $N = 200$; (c) $m = 0.1$, $N = 250$; (d) $m = 0.2$, $N = 100$; (e) $m = 0.2$, $N = 200$; (f) $m = 0.2$, $N = 250$; (g) $m = 0.3$, $N = 100$; (h) $m = 0.3$, $N = 200$; (i) $m = 0.3$, $N = 250$; (j) $m = 0.4$, $N = 100$; (k) $m = 0.4$, $N = 200$; (l) $m = 0.4$, $N = 250$.

Fig. 5 Interface damage of the components: (a) $m = 0.1$; (b) $m = 0.2$; (c) $m = 0.3$; (d) $m = 0.4$.

For components with a stress level of 0.3, the total strain loss increased rapidly at the beginning of the FT tests, with the growth rate rising exponentially after 50 FTCs. After approximately 100 FTCs, the FT damage accumulated, and the total strain loss exhibited unstable growth. The concrete frost heaving cracks penetrated, leading to premature failure of the component. For the stress level of 0.4, the total strain loss increased quickly before 50 FTCs, after which the loss rate accelerated drastically.

After 50 FTCs, the total strain loss at the end of components with stress levels of 0.1, 0.2, 0.3, and 0.4 increased by 1.56, 1.96, 15.55, and 3.51 times. After 300 FTCs, the loss in the middle of components with stress levels of 0.1 and 0.2 increased by 17.67 and 20.97 times, respectively.

4.3.3 Effects of stress levels

Figure 9 presents the variations of the total strain under different stress levels with FTCs. With increasing FTCs and stress levels, the total strain continuously descended, and the strain loss increased.

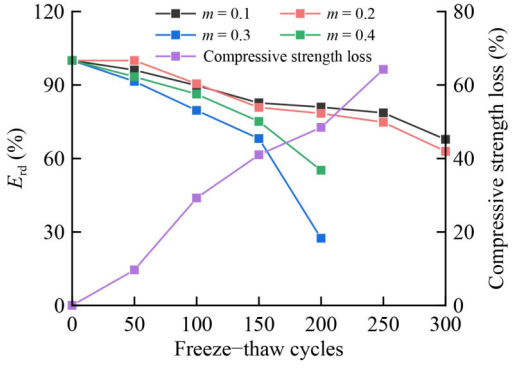

Fig. 6 Variations of concrete mechanical properties with FTCs.

For components with stress levels of 0.1 and 0.2, the total strain initially decreased slowly until the FTCs reached 250. After that, the rate of decline accelerated significantly. Components with stress levels of 0.3 and 0.4 exhibited two distinct stages: a slow decrease followed by a rapid decline. At the end and middle positions of the components, the total strain decreased sharply after 25 and 50 FTCs with a stress level of 0.3. And for a stress level of 0.4, the total strain rapidly declined after 50 and 100 FTCs.

After 100 FTCs, the strain at the end of the components with stress levels of 0.1, 0.2, and 0.4 decreased by 17.9%, 19.7%, and 34.2% of the total strain, respectively. After 250 FTCs, the mid-span strain loss of the components with stress levels of 0.1 and 0.4 lost 29.7% and 49.7% of the total strain.

4.3.4 Effects of the different locations

The variations of the total strain loss along the length of the components are shown in Fig. 10. It can be indicated that under the same FTCs, with increasing distance from the end of the components, the loss generally showed a decreasing trend at different stress levels.

For stress levels of 0.1 and 0.2, when the distance from the end of the components was less than 0.6 m, the loss fluctuated and decreased along the length of the

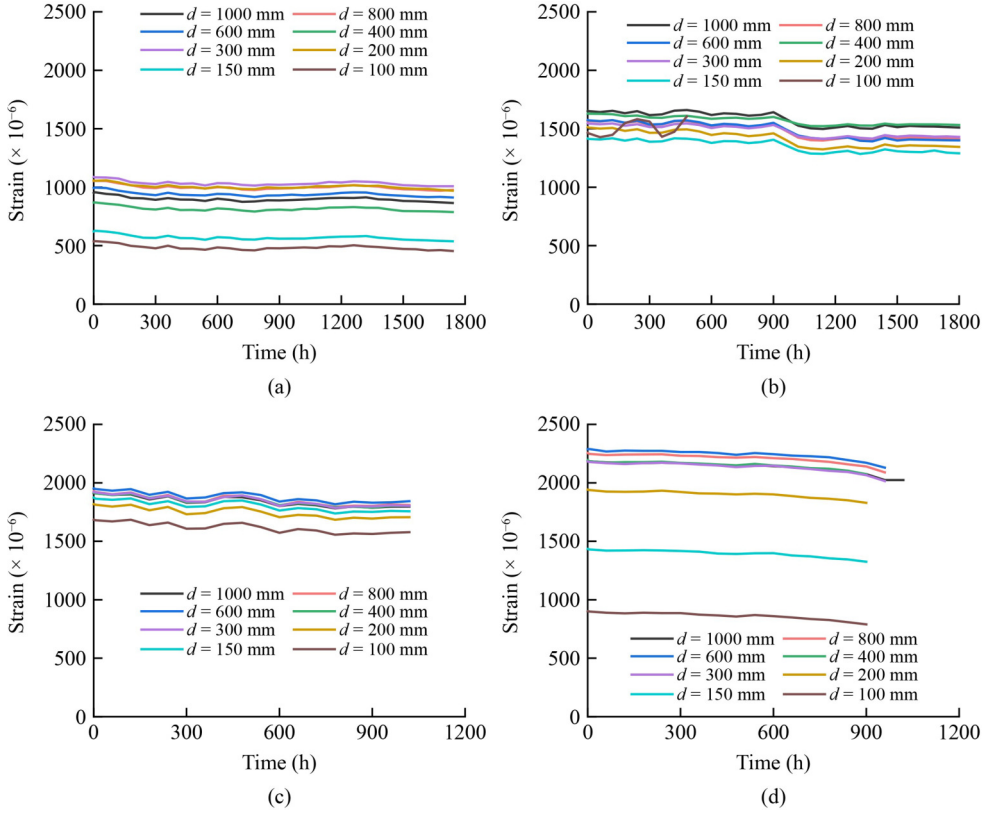

Fig. 7 Variations of the total strain with time for components without FT: (a) m = 0.1; (b) m = 0.2; (c) m = 0.3; (d) m = 0.4.

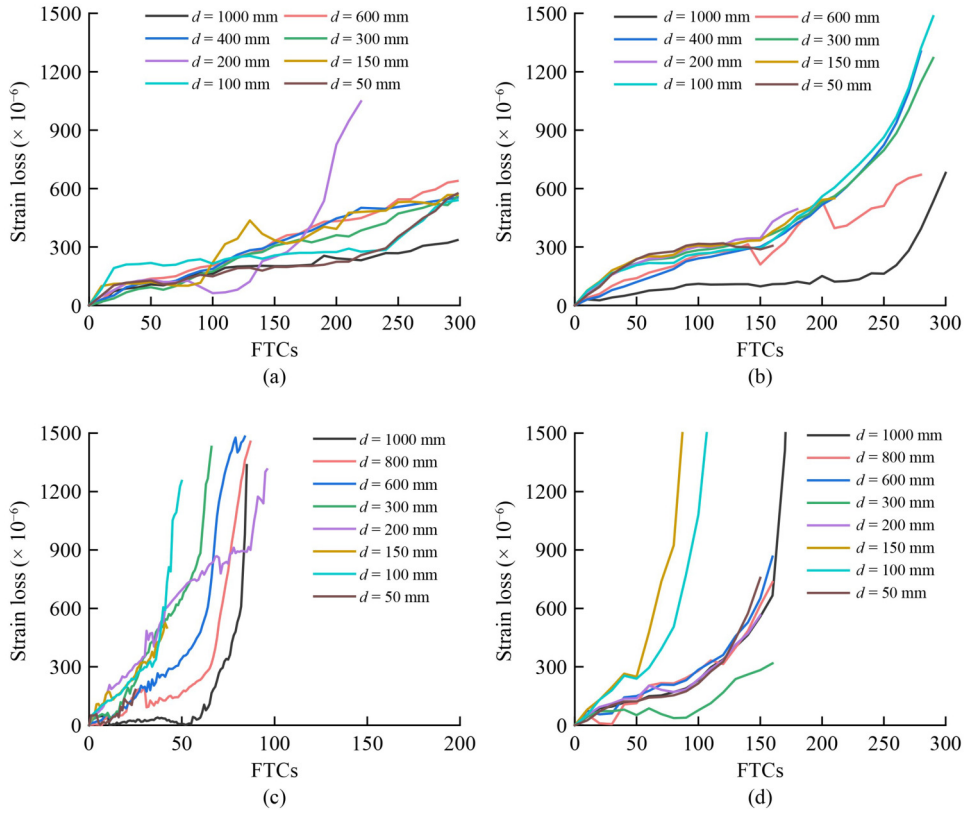

Fig. 8 Variations of the total strain loss at different positions with FTCs: (a) $m = 0.1$; (b) $m = 0.2$; (c) $m = 0.3$; (d) $m = 0.4$.

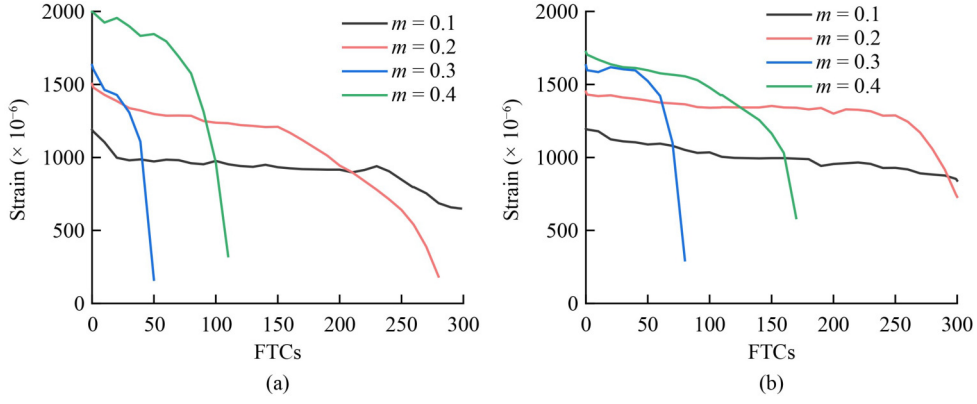

Fig. 9 Variations of the total strain under different stress levels with FTCs: (a) $d = 100$ mm; (b) $d = 1000$ mm.

components. When the distance exceeded 0.6 m, the loss continuously dropped, and the closer to the middle of the components, the smaller the loss.

For components with stress levels of 0.3 and 0.4, when the distance from the end was less than 0.6 m, the loss descended rapidly. When the distance surpassed 0.6 m, the loss dropped slowly as the distance increased.

After 150 FTCs, the mid-span loss of the components with stress levels of 0.1, 0.2, and 0.4 were 56.5%, 33.3%, and 18.1% of that at the end.

4.4 Analysis of concrete frost heaving strain

Figure 11 presents the variations of concrete frost heaving strain with temperature and time. It can be seen that the frost heaving strain continued to increase as the temperature decreased, and descended persistently as the temperature rose. During the low temperature constant stage, the FT damage of the components intensified over time, causing cracks on the concrete surface and a decrease in the frost heaving strain at a slow rate.

It was further found that the development of the frost heaving strain underwent four stages. In the first stage, as the temperature gradually decreased, the frost heaving strain ascended. The second stage was that at a constant low temperature, the frost heaving strain slowly declined over time. In the third stage, as the temperature rose from the lowest temperature to around 25 °C, the frost heaving

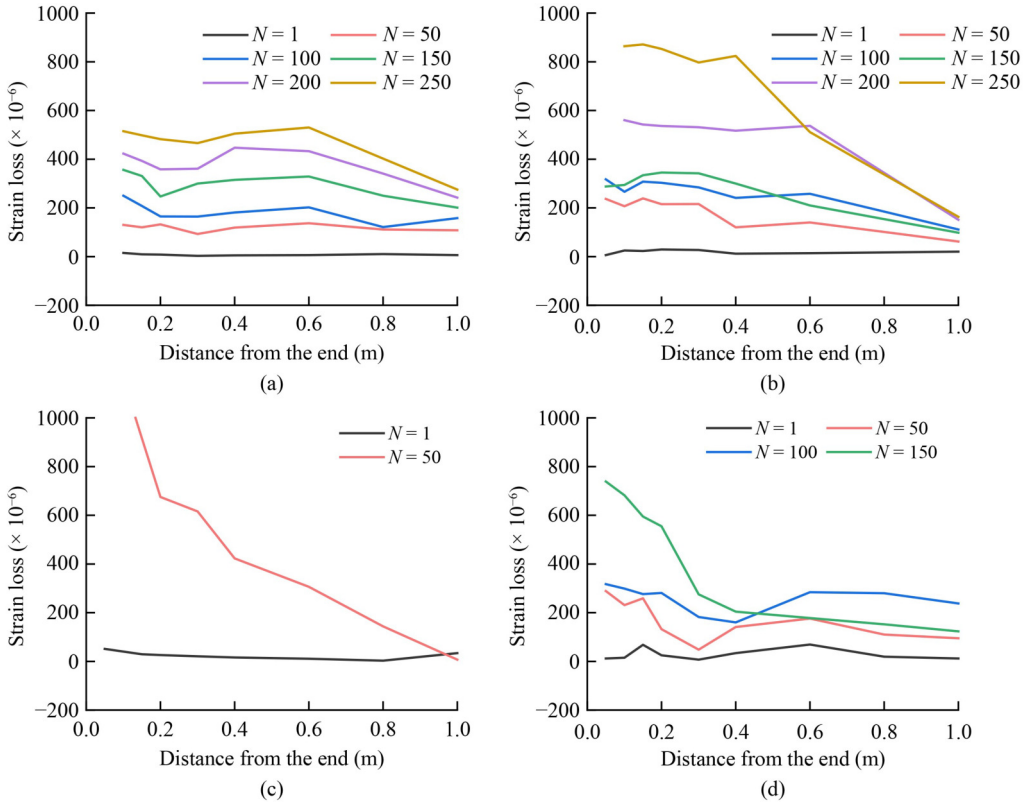

Fig. 10 Variations of the total strain loss along the length of the components: (a) m = 0.1; (b) m = 0.2; (c) m = 0.3; (d) m = 0.4.

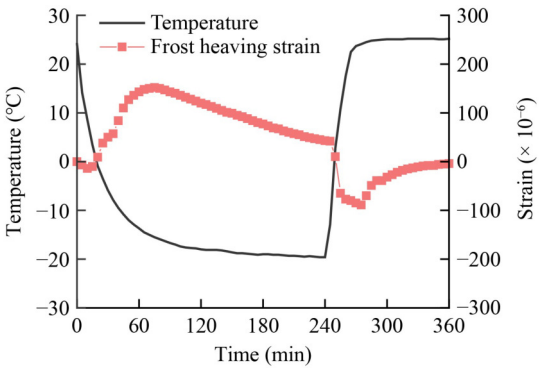

Fig. 11 Variations of the frost heaving strain with temperature and time.

strain sharply decreased with the increasing temperature. In the fourth stage, at around 25 °C, the frost heaving strain gradually increased.

4.4.1 Effects of freeze–thaw cycles

Figure 12 shows the variations of the frost heaving strain with time under different FTCs. With an increasing number of FTCs, the frost heaving strain under various stress levels increased. The higher the stress level, the larger the frost heaving strain.

After 50 FTCs, the peak frost heaving strain with stress levels of 0.1 to 0.4 increased by 30.3%, 24.6%, 59.9%, and 60.6%. After 150 FTCs, the peak frost heaving strain with stress levels of 0.1, 0.2, and 0.4 increased by 51.3%, 30.1%, and 61.5%, respectively. The component with a stress level of 0.3 failed after about 100 FTCs due to the excessively fast decrease in strain.

It was revealed that the frost heaving behavior of the concrete occurred repeatedly during FTCs. As the number of FTCs increased, the expansion of freezing water within the concrete's pores gradually enlarged cracks and disrupted the pore structure, resulting in an increase in frost heaving strain. This cumulative effect accelerated material deterioration over time.

4.4.2 Effects of stress levels

The variations of the frost heaving strain with time under different stress levels are shown in Fig. 13. It can be indicated that under the same FTCs, the peak frost heaving strain increased with the rise in stress levels. The more the number of FTCs, the larger the peak frost heaving strain. After 100 FTCs, the difference of frost heaving strain in different stress levels increased, and the dispersion of the curves became more noticeable.

When the FTCs were 50, compared to the component with a stress level of 0.1, the peak frost heaving strain with stress levels of 0.2, 0.3, and 0.4 increased by 11.1%,

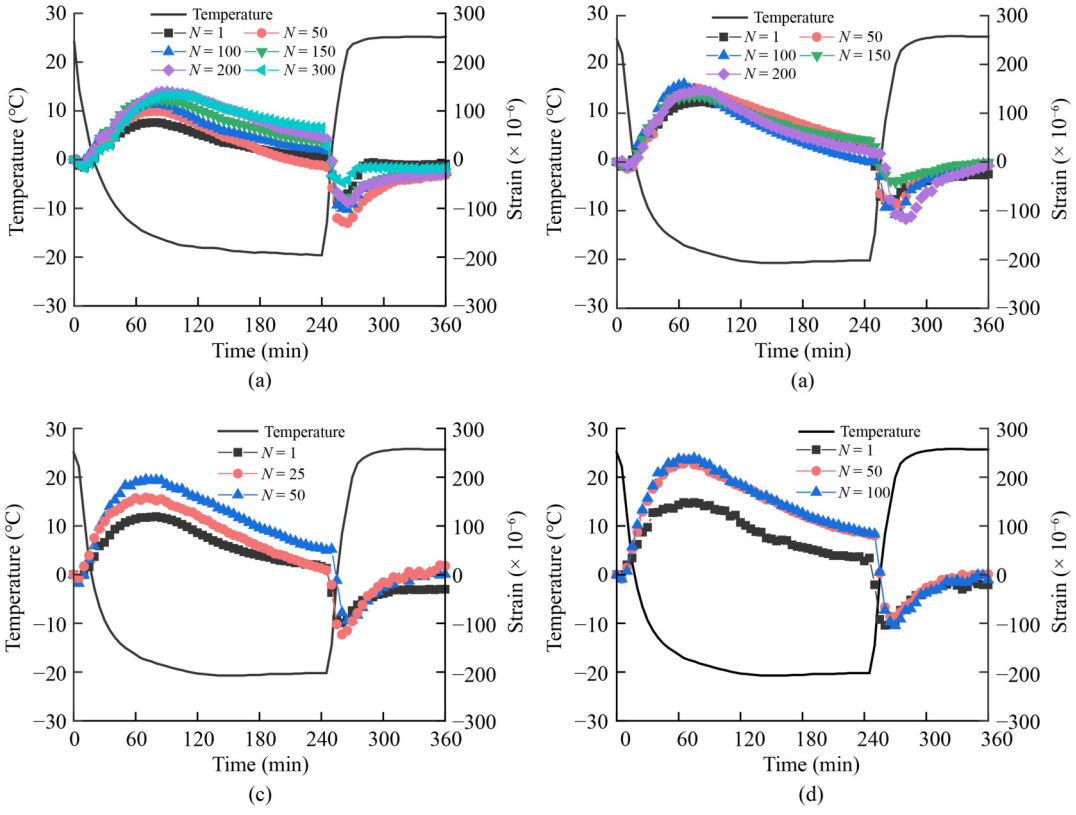

Fig. 12 Variations of the frost heaving strain with time under different FTCs: (a) m = 0.1; (b) m = 0.2; (c) m = 0.3; (d) m = 0.4.

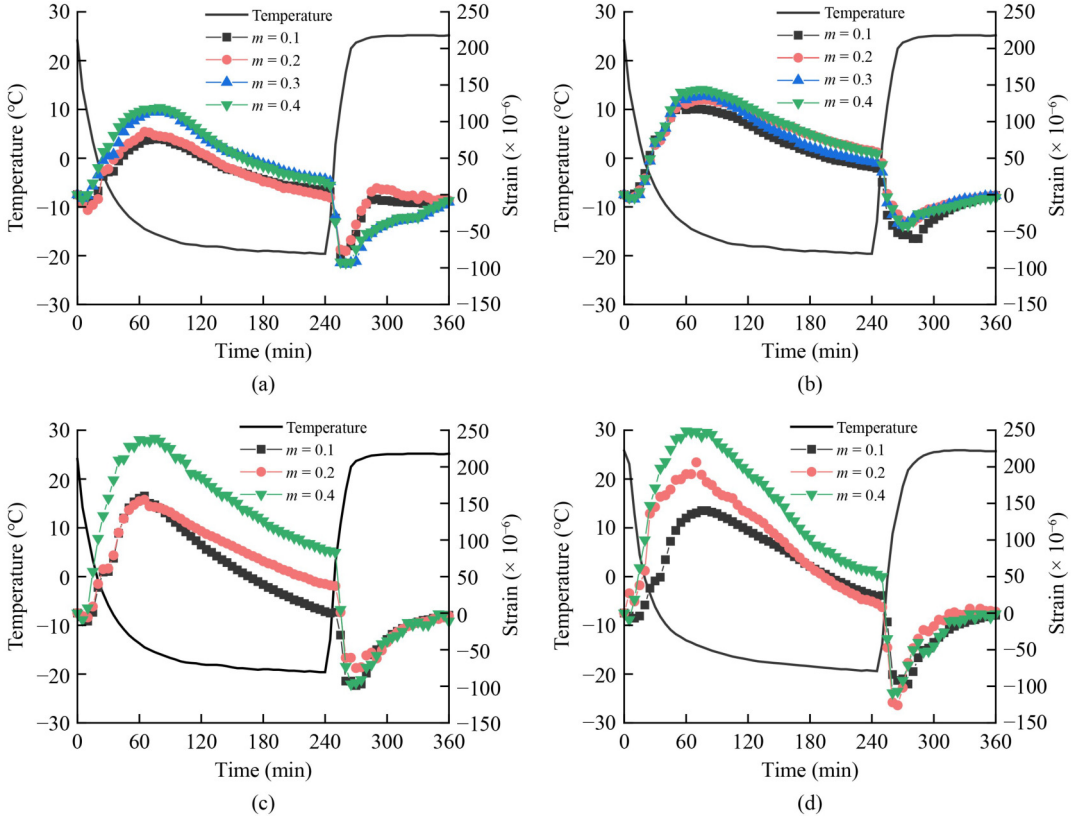

Fig. 13 Variations of the frost heaving strain with time under different stress levels: (a) N = 1; (b) N = 50; (c) N = 100; (d) N = 150.

15.4%, and 23.1%, respectively. After 150 FTCs, the peak frost heaving strain of the component with a stress level of 0.4 was 1.78 times and 1.31 times that with stress levels of 0.1 and 0.2, respectively.

The results indicated that low stress level led to an increase in the density of the concrete, which slightly inhibited the development of initial microcracks, resulting in minimal concrete damage during FTCs. However, at higher stress level, the combined effects of stress and frost heaving behavior accelerated crack propagation, leading to an increase in frost heaving strain.

4.4.3 Effects of the different locations

Figure 14 presents the hysteresis curves of the frost heaving strain at different locations of the component with a stress level of 0.1. It can be seen that with the increase in FTCs, the peak frost heaving strain rose, and the growth rate at the end of the component was faster than that at the middle.

After 100 FTCs, the frost heaving strain at the middle and end of the components increased by 78.9% and 103.9%, respectively. After 250 FTCs, the mid-span frost heaving strain of the component was 49.3% of that at the end.

It was because the end of the post-tension PC components was in a three-dimensional stress state and was subjected to a complex stress state. During the FTCs, the interface between the end concrete, the grout and the prestressing tendon was the first to be damaged. The FT damage at the end of the components was heavier than that at the middle, so the difference in the peak frost heaving strain between the two locations enlarged.

4.4.4 Analysis of the residual strain

The deformation caused by ice pressure during the FTCs included both elastic and plastic components. As the temperature gradually increased to room temperature during an FTC, the frost heaving strain decreased, and the elastic deformation was completely dissipated. The unrecovered plastic strain remained as residual frost heaving strain [36]. The accumulation of this residual strain could have led to the failure of localized regions of the structure, particularly in the weaker areas of the concrete.

The difference in frost heaving strain at the lowest temperature between the two FTC curves was used as the residual strain of the components. Figure 15 shows the variations of residual strain with FTCs. It can be observed

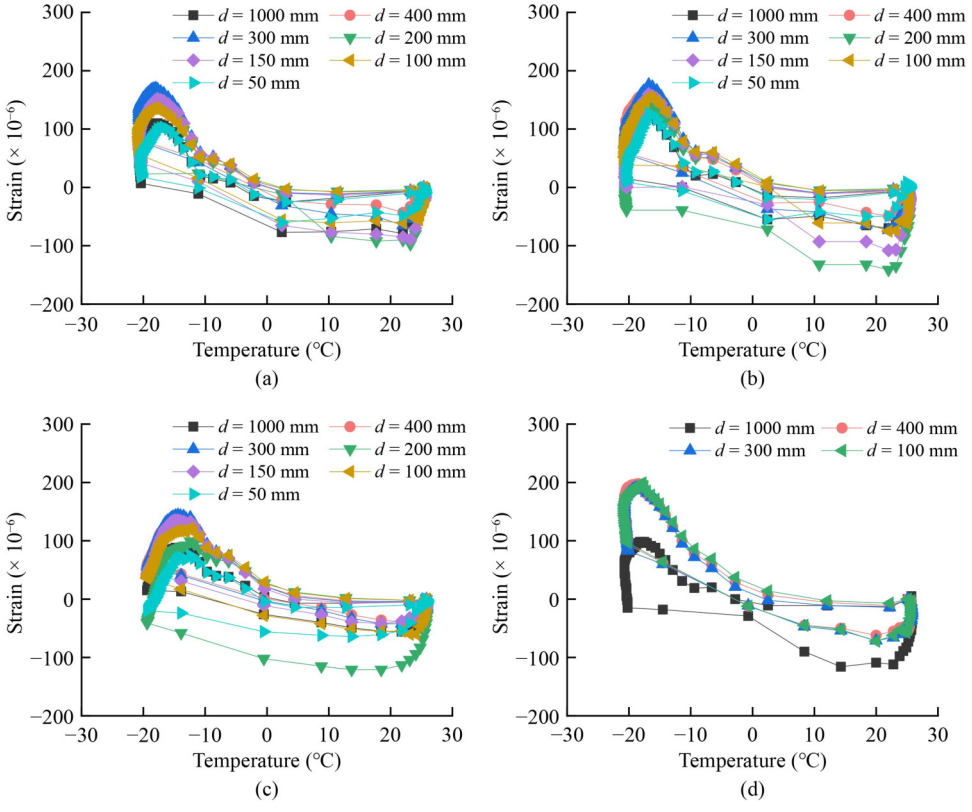

Fig. 14 Hysteresis curves of the frost heaving strain at different locations of the components: (a) $N = 50$; (b) $N = 100$; (c) $N = 150$; (d) $N = 250$.

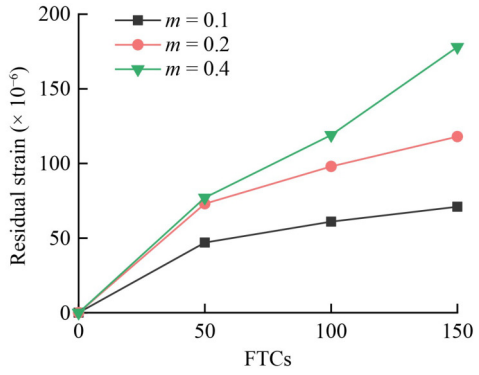

Fig. 15 Variations of the residual strain with FTCs.

that as the FTCs increased, the residual strain curves at various stress levels exhibited an upward trend. The higher the stress level, the larger the residual strain.

Before 50 FTCs, the residual strain increased rapidly; after 50 FTCs, the growth rate of residual strain declined. When FTCs ascended from 50 to 150, the residual strain with stress levels of 0.1, 0.2, and 0.4 increased by 51.1%, 61.6%, and 131.2%, respectively.

5 The strain loss model of prestressed concrete components under freeze–thaw cycles

5.1 The proposed model

The stress level of the concrete is m, the concrete prestress force F_0 and compressive strain ε_0 can be calculated by Eqs. (5) and (6)

$$F_0 = mf_{ck}^0 A_n, \tag{5}$$

$$\varepsilon_0 = \frac{F_0}{A_n E_c(0)}, \tag{6}$$

where $f_{ck}^{\ 0}$ is the axial compressive strength of the unfrozen concrete, MPa; A_n is the net cross-sectional area of the concrete, mm^2; $E_c(0)$ is the dynamic modulus of elasticity of the unfrozen concrete, MPa.

After N FTCs, the concrete prestress force F_N and compressive strain ε_N can be calculated by Eqs. (7) and (8)

$$F_N = F_0 - A_p E_p \Delta\varepsilon, \tag{7}$$

$$\varepsilon_N = \frac{F_N}{A_n E_c(N)}, \tag{8}$$

where E_p is the modulus of elasticity of the prestressing tendon, MPa; A_p is the cross-sectional area of the prestressing tendon, mm^2; $E_c(N)$ is the dynamic modulus of elasticity of the concrete after N FTCs, MPa.

The total strain loss of the prestressing tendon after N FTCs can be expressed as

$$\Delta\varepsilon = \varepsilon_0 - \varepsilon_N = mf_{ck}^0 A_c \frac{E_c(N) - E_c(0)}{\{A_c E_c(N) + E_p A_p\} E_c(0)}. \tag{9}$$

During the FT tests, concrete suffered damage and its dynamic modulus of elasticity changed. To characterize the FT deterioration of the components, the damage was defined as E_{rd}, which can be calculated by Eq. (2).

After N FTCs, the dynamic modulus of elasticity of FT damaged concrete can be calculated by Eq. (10)

$$E_c(N) = E_c(0) E_{rd}. \tag{10}$$

By substituting Eq. (10) into Eq. (9) and introducing parameter A for model correction, the final theoretical model of the strain loss is shown in Eq. (11). The FTCs and stress levels were taken into account in this model.

$$\Delta\varepsilon = Amf_{ck}^0 A_c \frac{(1 - E_{rd})}{\{A_c E_c(0) E_{rd} + E_p A_p\}}. \tag{11}$$

5.2 Verification of the proposed model

According to Eq. (2), the E_{rd} under different FTCs could be calculated and was fitted with a quadratic polynomial with the FTCs to obtain the related function. The fitting result is shown in Fig. 16.

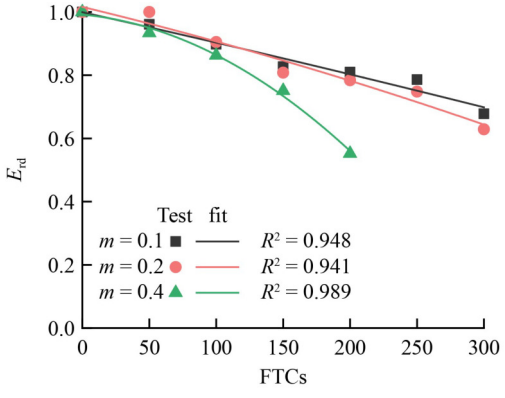

Fig. 16 Fitted curves for the relationship between E_{rd} and FTCs.

The obtained polynomial fitting curve equation and related parameters were substituted into Eq. (11) to get the final theoretical model. The comparison of the theoretical model and experimental data are shown in Fig. 17. Based on the fitting results of the model, it could be concluded that the calculated strain loss had a good fitting effect with the experimental data. It was indicated that the model was reasonable.

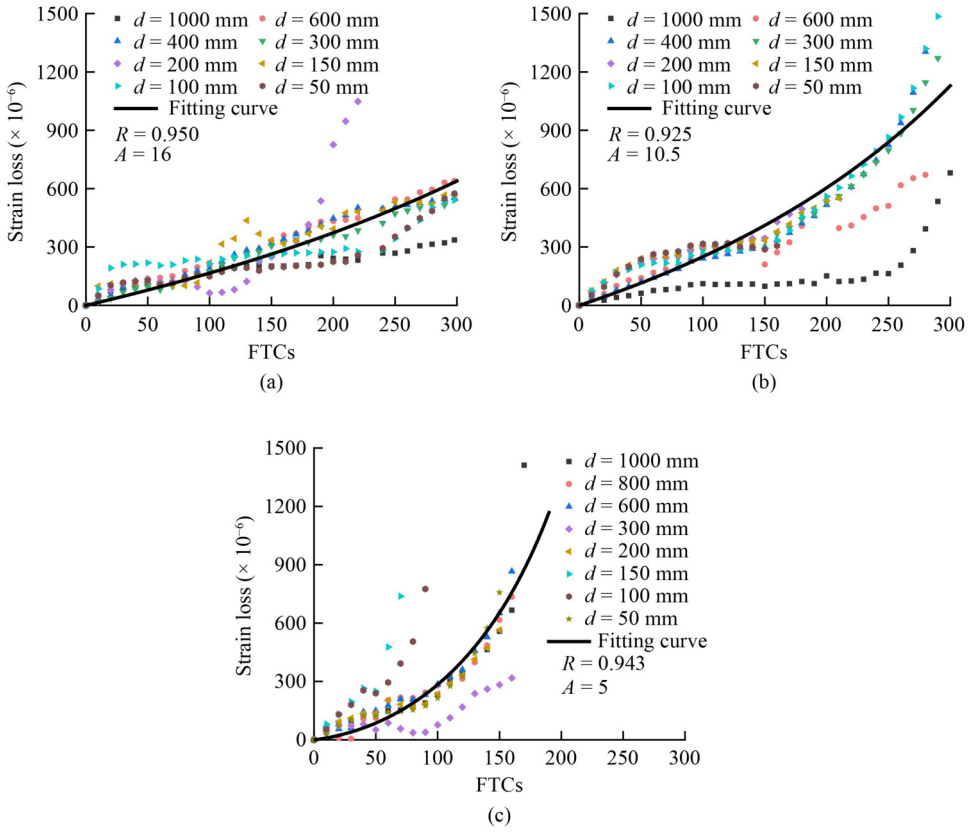

Fig. 17 Comparison between the experimental data and theoretical model: (a) $m = 0.1$; (b) $m = 0.2$; (c) $m = 0.4$.

6 Conclusions

This article presented an experimental study on the frost heaving failure and the strain behavior of PC components under FTCs. The following achievements have been obtained.

1) The total strain of the prestressing bras decreased with the increase in FTCs, the strain loss ascended with increasing stress levels, and the deceleration rate at the end of the components was faster than that at the middle. After 300 FTCs, the mid-span strain loss of components with stress levels of 0.1 and 0.2 increased by 17.67 and 20.97 times, respectively.

2) As FTCs increased, the peak frost heaving strain ascended. As the stress level rose, the effect of prestress forces on the concrete frost cracking from inhibition switch to aggravation. After 150 FTCs, the peak frost heaving strain of the component with a stress level of 0.4 was 1.78 times and 1.31 times that with stress levels of 0.1 and 0.2, respectively.

3) The total strain loss model for PC components was established, considering the influence of FTCs and stress levels, and it was acceptable with experimental results.

Acknowledgements The present study was sponsored by the National Natural Science Foundation of China (Grant Nos. 52178163 and 51808437), Xi'an Science and Technology Plan (No. 22SFSF0005), the Key R&D Program of Shaanxi Province (No. 2022SF-403), the China Scholarship Council (No. 201908610062), and Shaanxi Science Fund for Distinguished Young Scholars (No. 2018JC-025).

Competing interests The authors declare that they have no competing interests.

References

1. Liu D Y, Tu Y M, Sas G, Elfgren L. Freeze–thaw damage evaluation and model creation for concrete exposed to freeze–thaw cycles at early-age. Construction & Building Materials, 2021, 312: 125352
2. Yu H F, Ma H X, Yan K. An equation for determining freeze–thaw fatigue damage in concrete and a model for predicting the service life. Construction & Building Materials, 2017, 137: 104–116
3. Ebrahimi K, Daiezadeh M J, Zakertabrizi M, Zahmatkesh F, Habibnejad Korayem A. A review of the impact of micro-and nanoparticles on freeze–thaw durability of hardened concrete: Mechanism perspective. Construction & Building Materials, 2018, 186: 1105–1113
4. Deng Y, Gui J Y, Zhang H X, Taliercio A, Zhang P, Wong S H F, Sukontasukkul P, Khan A, Li L, Tang Y C, et al. Study on crack width and crack resistance of eccentrically tensioned steel-reinforced concrete members prestressed by CFRP tendons. Engineering Structures, 2022, 252: 113651
5. Qin X C, Meng S P, Cao D F, Tu Y M, Sabourova N, Grip N, Ohlsson U, Blanksvärd T, Sas G, Elfgren L. Evaluation of freeze–thaw damage on concrete material and prestressed concrete

specimens. Construction & Building Materials, 2016, 125: 892–904
6. Sun B L, Yang Y Q, Li X B, Yan M, Xie M Z, Bao Y. Full-scale investigation of post-tensioned prestressed concrete bridge girders subjected to frost heaving in cold regions. Engineering Structures, 2022, 250: 113413
7. Lin H W, Han Y F, Liang S M, Gong F Y, Han S, Shi C W, Feng P. Effects of low temperatures and cryogenic freeze–thaw cycles on concrete mechanical properties: A literature review. Construction & Building Materials, 2022, 345: 128287
8. Wang R J, Zhang Q J, Li Y. Deterioration of concrete under the coupling effects of freeze–thaw cycles and other actions: A review. Construction & Building Materials, 2022, 319: 126045
9. Zhang W H, Pi Y L, Kong W P, Zhang Y S, Wu P P, Zeng W Z, Yang F H. Influence of damage degree on the degradation of concrete under freezing–thawing cycles. Construction & Building Materials, 2020, 260: 119903
10. Cui W, Liu M M, Wang L X, Guan W, Song H F, Li F. Experimental study on deterioration characteristics of prestressed concrete under the coupling of freeze–thaw and corrosion. Journal of Materials in Civil Engineering, 2022, 34(2): 04021447
11. Xie J, Zhao X Q, Yan J B. Experimental and numerical studies on bonded prestressed concrete beams at low temperatures. Construction & Building Materials, 2018, 188: 101–118
12. Cao D F, Qin X C, Meng S P, Tu Y M, Elfgren L, Sabourova N, Grip N, Ohlsson U, Blanksvärdet T. Evaluation of prestress losses in prestressed concrete specimens subjected to freeze–thaw cycles. Structure and Infrastructure Engineering, 2016, 12(2): 159–170
13. Li C, Yang L B, Luo C, Liu H, Wan X R. Frost heaving strain monitoring for lining structure in extreme cold and high-altitude area with FBG strain sensors. Measurement, 2022, 196: 110918
14. Lv H F, Kong X L, Ren J, Zhao X F, Sun C S. Research on real-time monitoring of strain behavior of concrete under freezing–thawing cycle by white light interferometer. Advances in Materials Science and Engineering, 2022, 2022(1): 8049092
15. Fu W W, Sun B C, Wan H P, Luo Y Z, Zhao W J. A Gaussian processes-based approach for damage detection of concrete structure using temperature-induced strain. Engineering Structures, 2022, 268: 114740
16. Zhao Y, Lian S L, Bi J, Wang C L, Zheng K. Study on freezing–thawing damage mechanism and evolution model of concrete. Theoretical and Applied Fracture Mechanics, 2022, 121: 103439
17. Wang R J, Hu Z Y, Li Y, Wang K, Zhang H. Review on the deterioration and approaches to enhance the durability of concrete in the freeze–thaw environment. Construction & Building Materials, 2022, 321: 126371
18. Lu Z, She J B, Wu X W, Yao H L. Cumulative strain characteristics of compacted soil under effect of freeze–thaw cycles with water supply. Transportation Geotechnics, 2019, 21: 100291
19. Sun B C, Fu W W, Luo Y Z, Zhao W J. Development of internal moisture transfer and cumulative residual strain in concrete under freeze–thaw cycle. Journal of Materials Research and Technology, 2022, 20: 1243–1254
20. Lv H F, Liao K X, Kong X L, Zhao X F, Sun C S. Monitoring the residual strain of concrete in a freezing–thawing environment using white light interferometer. Cold Regions Science and Technology, 2017, 142: 132–138
21. Zhao X F, Lv X J, Wang L, Zhu Y F, Dong H, Chen W, Li J K, Ji B, Ding Y B. Research of concrete residual strains monitoring based on WLI and FBG following exposure to freeze–thaw tests. Cold Regions Science and Technology, 2015, 116: 40–48
22. Mu L J, Wang L C, Wang L. Investigation on water absorption of concrete under the coupling action of uniaxial compressive load and freeze–thaw cycles. Materials and Structures, 2022, 55(4): 127
23. Xu Y Q, Ye H S, Yuan Q, Shi C J, Gao Y, Fu Q. The durability of concrete subject to mechanical load coupled with freeze–thaw cycles: A review. Archives of Civil and Mechanical Engineering, 2022, 22(1): 47
24. Wang B X, Wang F, Wang Q. Damage constitutive models of concrete under the coupling action of freeze–thaw cycles and load based on Lemaitre assumption. Construction & Building Materials, 2018, 173: 332–341
25. Yuan Y, Zhao R D, Li R, Wang Y B, Cheng Z Q, Li F H, John Ma Z. Frost resistance of fiber-reinforced blended slag and Class F fly ash-based geopolymer concrete under the coupling effect of freeze–thaw cycling and axial compressive loading. Construction & Building Materials, 2020, 250: 118831
26. Wang Y R, Cao Y B, Zhang P, Ma Y W, Zhao T J, Wang H, Zhang Z H. Water absorption and chloride diffusivity of concrete under the coupling effect of uniaxial compressive load and freeze–thaw cycles. Construction & Building Materials, 2019, 209: 566–576
27. Shen Y, Liu J, Zhou S Y, Li G P. Experimental investigation on the freeze–thaw durability of concrete under compressive load and with joints. Construction & Building Materials, 2019, 229: 116893
28. Liu K H, Yan J C, Meng X X, Zou C Y. Bond behavior between deformed steel bars and recycled aggregate concrete after freeze–thaw cycles. Construction & Building Materials, 2020, 232: 117236
29. GB/T 50448-2015. Technical Code for Application of Cementitious Grout. Beijing: Ministry of Housing and Urban-Rural Development of the People's Republic of China, 2015
30. GB/T 50082-2009. Standard for Test Methods of Long-Term Performance and Durability of Ordinary Concrete. Beijing: Ministry of Housing and Urban-Rural Development of the People's Republic of China, 2009
31. CECS21-2000. Technical Specification for Inspection of Concrete Defects by Ultrasonic Method. Beijing: China Association for Engineering Construction Standardization, 2000
32. Gonen S, Soyoz S. Investigations on the elasticity modulus of stone masonry. Structures, 2021, 30: 378–389
33. Lv Z T, Xia C C, Wang Y S, Lin Z. Frost heave and freezing processes of saturated rock with an open crack under different freezing conditions. Frontiers of Structural and Civil Engineering, 2020, 14(4): 947–960
34. Zhao J, Li K, Li H, Li A, Xi C. Research on the thermal conductivity of C/C composites. Acta Aeronautica et Astronautica Sinica, 2005, 26(4): 501–504 (in Chinese)
35. Liu X G, Lei Y J, Sun Y H, Zhou J L, Niu D T. Influence of freeze-thaw damage gradient on stress–strain relationship of stressed concrete. Frontiers of Structural and Civil Engineering, 2023, 17(9): 1326–1340
36. Xia C C, Cao S P, Zhou S W, Li X Y, Duan J Z. Nonuniform frost heave of saturated porous rocks in cold regions during cyclic unidirectional freeze–thaw: Influence of the temperature gradient. Bulletin of Engineering Geology and the Environment, 2024, 83(9): 365